Available online at www.sciencedirect.com

ScienceDirect

journal homepage: http://www.elsevier.com/locate/rpor

Original research article

Calculation and measurement of doses in the surface layers of a phantom when using Tomotherapy

Anna Kowalik[a,*], *E. Konstanty*[a], *Tomasz Piotrowski*[a,b], *Malgorzata Skórska*[a], *Julian Malicki*[a,b]

[a] *Department of Medical Physics, Greater Poland Cancer Centre, Garbary 15, Poznan, Poland*
[b] *Department of Electroradiology, University of Medical Sciences, Poznan, Poland*

ARTICLE INFO

Article history:
Received 1 July 2018
Received in revised form
27 November 2018
Accepted 30 November 2018
Available online 1 March 2019

Keywords:
Tomotherpy
Thermoluminescence dosimetry
Doses in the skin

ABSTRACT

Background: The calculation and measurement on the surface of the skin presents a significant dosimetric problem because of numerous factors which have an influence on the dose distribution in this region.
Aim: The overall aim of this study was to check the agreement between doses measured with thermoluminescent detectors (TLD) during tomotherapy photon beam irradiation of the skin area of a solid water cylindrical phantom with doses calculated with Hi-Art treatment planning system (TPS).
Material and Method: The measurements of the dose were made with the use of a solid water cylindrical phantom - Cheese Phantom. Two bolus phantoms were used: 5 mm and 10 mm Six different planning treatments were generated. The doses were measured using TL detectors.
Results: In the case of a tumor located near the surface of the skin, the mean dose for 0.5 cm bolus was - 1.94 Gy, and for 1 cm bolus - 2.03 Gy. For the tumor located inside the phantom and organ at risk on the same side that TL detectors, for a 0.5 cm bolus, mean dose was 0.658 Gy, and for a 1 cm bolus, 0.62 Gy.
Conclusion: The analysis of results showed that the relative percentage difference between measured and planned dose in the field of irradiation was less than 10%, while the largest differences were on the board of the field of radiation and outside of the field of irradiation, where the dose was 0.08 Gy to 1 Gy.

1. Introduction

Radiotherapy is an oncological treatment that uses specific properties of ionizing radiation to interact with living cells. This method is used for both radical treatment, which is intended to completely cure the patient, and palliative

* *Corresponding author.*
E-mail address: annakowalik@poczta.onet.pl (A. Kowalik).
https://doi.org/10.1016/j.rpor.2018.11.006

treatment, which aims to inhibit the disease process and reduce the discomfort in the case of disseminated tumor lesions, as well as symptomatic treatment.

Radiotherapy for the delivery of a dose to the tumor is divided into:

Teleradiotherapy – where the radiation source is a linear accelerator or radioactive isotope located at a certain distance from the patient,

Brachytherapy – where the source of radiation is a radioactive isotope located in direct contact with the tumor.[1]

The continuous development of radiotherapy methods increasingly demands the use of therapeutic medical equipment. Modern technologies, starting with particle accelerators, intensive dose modulation techniques (IMRT), imaging techniques (IGRT), or tomotherapy, allow more conformational tumor dose distribution. The consequence of the conformation of doses in a tumor volume is dose reduction in critical organs. Tomotherapy is a spiral irradiation technique, so it is difficult to achieve a homogeneous dose distribution in the skin. On the basis of literature, it can be demonstrated that there is no documented methodology or any reliable results for measuring and verifying dose in the surface layers of the skin. It is, therefore, necessary to undertake a study to make it possible to specify a method of measuring doses in the skin, which is difficult due to many factors. There are a few publications on this subject. Martin J. Buton, Tsang Cheung, Peter Yu and Peter Netcalfe in their paper entitled "Effects on skin dose from unwanted air gaps under bolus in photon beam radiotherapy" attempted to assess the effect of airspots underneath the bolus during patient irradiation on a classical Linear accelerator.[2] The article entitled "Skin dose study of chest wall treatment with Tomotherapy" attempted to assess the dose distribution on the skin during thoracic irradiation on a classic accelerator and Tomotherapy. Tangential technology is often a challenge in achieving uniformity of dosage in irradiated volume. Tissue-like bolus is often used to provide the right dose. Tomotherapy is a technique of irradiation that allows a homogeneous dose distribution in PTV. Authors in this experiment hypothesized that getting the right dose on the skin while irradiating the chest wall on Tomotherapy will not require a bolus. The study compared the doses to the skin during irradiation on a tomotherapeutic device and on a classic linear accelerator.[3] Kim et al. in their study described the dose distribution near the surface during irradiation on Tomotherpay. In the article "Superficial Dosimetry for Helical Tomotherapy", we investigated the effect of radiation delivery during spiral tomotherapy on the skin.[4]

2. Aim

The general aim of the work was to do dosimetric verification of the calculation algorithm of doses in surface layers of a tissue-like phantom during irradiation of tumor lesions with spiral Tomotherapy.

The most important specific objective was to define the radiographic parameters of the spiral Tomotherapy accelerator – Cheese phantom to obtain a desired dose distribution. A very strong emphasis was put in this study to develop a method of calibration of thermoluminescent detectors using spiral Tomotherapy.

One of the main points was the measurement and analysis of doses in surface layers of a tissue-like phantom corresponding to the surface layers of the skin by means of thermoluminescent detectors and the comparison of measured doses in surface layers of a Cheese phantom with dose distribution calculated in the treatment planning system for spiral tomotherapy.

3. Material

3.1. *Cheese phantom*

A phantom is a material either solid or liquid of a certain density that is close to the density of water or human tissue, which makes it possible to estimate the dose distribution in a biological medium without involving the patient. Due to the specificity of measurements, it is important to choose the right phantom shape and dimensions.

The Cheese Phantom was used to measure the dose in the surface layers of a phantom like phantom reflecting surface layers of the skin. The Cheese Phantom has a cylindrical shape with a diameter of 30 cm, height of 18 cm and is made up of two identical halves. Between these two components, it is possible to place an X-ray film. On one wall of the phantom, there are openings of 0.5 cm for the placement of ionization chambers, and the other wall has densities imitating different densities that allow the quality of images obtained using the MVCT detector to be evaluated. The average phantom density is 1.018 g/cm^3. Fig. 1 shows the Cheese Phantom in two views: front and rear.

3.2. *Thermoluminescence detectors*

Harshaw TL100 thermocoluminescence detectors from Harshaw are used in this work which are solid lithium fluoride (LiF) measuring $3.0 \times 3.0 \times 0.9$ mm. Lithium Fluoride stores electrons by trapping some of the energy absorbed while passing through the ionizing radiation. As a result of the sample heating, electrons are transferred from electron traps to higher levels where they then return to the basal level emitting energy in the form of light. The amount of energy absorbed by the detector that is emitted in the form of light is proportional to the number of electrons in the electron traps, which corresponds to the energy absorbed during irradiation. The absorbed charge reading is carried out in the reader of the thermoluminescent detectors which consists of a heater; photomultiplier processing a small amount of light per current pulse; counting system and microprocessor for pulse processing. After reading, the detector is thermally treated to prepare it for the next exposure. The sensitivity of the thermoluminescent detector is not constant and it is, therefore, necessary to perform calibration under appropriate conditions, which allows the calibration factor to be determined.

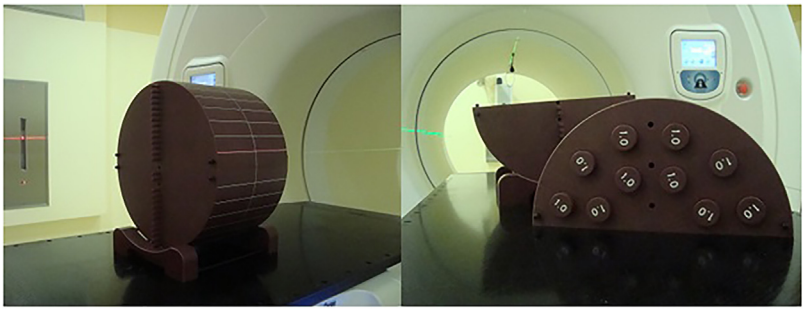

Fig. 1 – Cheese Phantom used for measuring dose on the surface of the skin using a tomotherapeutic apparatus. (A) shows a front view with locations for measuring the ionization chamber, while (B) shows a rear view with density peaks and the space for the ionization chamber.

3.3. *Phantom for calibration thermoluminescent detectors*

For the calibration of thermoluminescent detectors, a cylindrical shape phantom made of plastic such as Plexiglas is used, the main component of which is polymer - poly (methyl methacrylate). Phantom shape and density are similar those of the Cheese Phantom. Phantom is 30 cm in diameter and 30 cm in height. In the central part, there is a square plate made of Plexiglas just like the rest of the phantom, which made it possible to place the detectors in the central part of the phantom. The plate has dimensions of 11.8 cm × 11.8 cm and thickness of 2.4 cm. The phantom volume was 5645.25 cc, and the phantom mass was about 5700 g. The average phantom density was calculated to be 1.010 g/cc.

3.4. *Ionization chamber*

An A1SL ionization chamber was used to measure the dose in water, air and other phantoms. It is a sensitive method of measuring dose at a point. The A1SL Thimble Chamber is a thin-walled version of the A1. It has the same internal dimensions and volume as the A1 model, the entire chamber has a fixed diameter of 6.4 mm (0.250″) which is ideal for small phantoms. Small dosimetric measurements of 6 mm × 8 mm size Waterproof construction allows the use of a phantom dosing chamber in a water phantom. The chamber is located in a duct that surrounds a triaxial cable that provides a balance of pressure inside the chamber with the environment. Symmetrical construction of the ionization chamber makes it possible to uniformly collect the signal.[5]

4. Methods

4.1. *Calibration of TLD detectors*

The thermoluminescent detectors used for the tests show some differences. In response, it is therefore necessary to determine the calibration factor for each detector used. Calibration of the detectors consists in determining the response of a single detector to a given dose (in this case 2 Gy). The ratio of the set dose to the detector reading is called the Element Correction Coefficient (ECC). This factor is used to calculate the dose in the area of interest by multiplying the load reading from a single detector by that factor.

Table 1 – Conditions for calibration of thermoluminescent detectors on tomotherapy unit.

Photon energy	6 MV
Wide of the field	5.0 cm
Pitch	0.287
Planned modulation factor (actual)	2500 (2501)
Dose	2 Gy
Table speed	0.029 m/s

The detector calibration was performed using a 6 MV MV photon radiation on a Tomotherapy unit. Tomotherapy calculated the time of irradiation with the help of the treatment planning system to give a dose of 2 Gy (5 fractions of 2 Gy). Table 1 describes the conditions under which detectors were calibrated.

Phantoms prepared for calibration on tomotherapy were used for the calibration of thermoluminescent detectors. Phantom shape and density is similar to those of the Cheese Phantom. Phantom dimensions are: diameter 30 cm and height 30 cm.

In the central part, there is a square plate for placing the detectors. Fig. 2 shows the measurement system used for the calibration of thermoluminescent detectors.

Fig. 2 shows the dose distribution in the phantom used to calibrate the thermoluminescent detectors.

The central part of the phantom was a plate made of Plexiglas with the same density as the phantom, which contained 70 calibration detectors. The location of the detectors was a target where a homogeneous 2 Gy dose distribution was obtained.

The reading of the signal that was converted to dose was carried out in a Harshaw 3500 TLD Reader. The reading was made for a baking curve with a maximum temperature of 300 °C. Each time after reading the doses, the detectors were subjected to the final heating in a PTW-TLD oven at 400 °C for one hour followed by four hours at 100 °C. The calibration procedure was repeated five times, resulting in 37 out of 70 particle detectors on the skin surface.

4.2. *Calculation of dose distributions*

The first step was to perform a Cheese Phantom scan on a computerized tomography using a bolus of two different

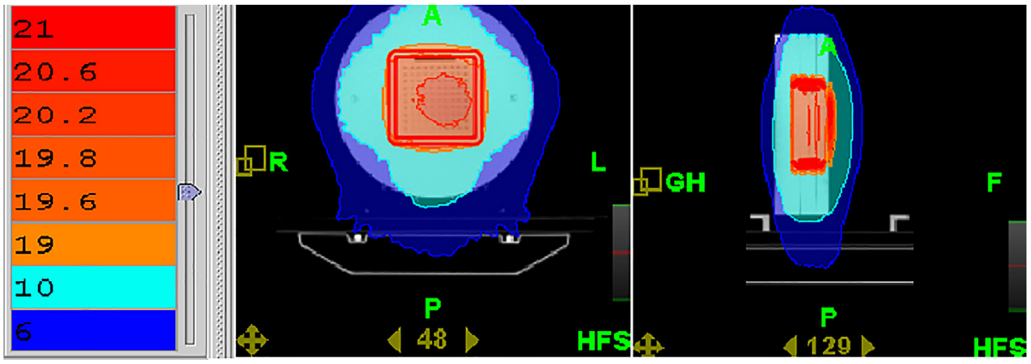

Fig. 2 – Calculated dose distribution in phantom for calibration of TLD detectors.

thicknesses. Bolus was located on the surface of the phantom. The phantom was scanned twice, first a 0.5 cm bolus was used; then, a bolus of 1 cm in thickness. In order to obtain accurate reconstruction of the image that is necessary for the execution of the treatment plans, the distance between the individual scans was determined at 3 mm.

After receiving the reconstructed images, three different tumor lesions and critical organs were identified in the phantom. In all six cases, the dose was 10 Gy in 5 fractions of 2 Gy. The field width was 2.5 cm for all cases, and the pitch was the same and amounted to 0.287. The planned modulation factor in all six cases considered was 2500. However, the actual coefficient was different for each of them. Table speed, duration of administration, and time of administration of fractions in MU varied depending on the clinical case.

4.3. *Six clinical cases of different tumor sites were considered*

1) Clinical case 1: 0.5 cm displacement at the skin surface with 0.5 cm of tissue-like bolus: the average skin surface dose was 1.38 Gy per fraction, the minimum dose was 0.12 Gy, The maximum dose was 1.94 Gy.
2) Clinical case 2: tumor of approx. 0.5 cm at the skin surface with 1 cm of tissue-like bolus: the average skin surface dose was 1.5 Gy per fraction, the minimum dose was 0.12 Gy, the maximum dose was 2.03 Gy.
3) Clinical case 3: a tumor located within the tissue-like phantom, where the critical organ was on the same side as the thermoluminescent detectors using a 0.5-cm tissue-like bolus: minimum dose 0.07 Gy, the maximum dose was 0.75 Gy.
4) Clinical case 4: a tumor located within the tissue-like phantom, where the critical organ was on the same side as the thermoluminescent detectors with 1 cm tissue-like bolus: the average skin surface dose was 0.555 Gy per fraction, the minimum dose was 0.073 Gy, the maximum dose was 0.790 Gy.
5) Clinical case 5: a tumor located within a tissue-like phantom, where the critical organ was on the opposite side of the thermoluminescent detector using a 0.5-cm tissue-like bolus: the average skin dose was 0.38 Gy per fraction, the maximum dose was 0.66 Gy.
6) Clinical case 6: tumor localized within the tissue-like phantom, where the critical organ was on the opposite side of the thermoluminescent detector with 1 cm of tissue-like bolus: the average skin surface dose was 0.43 Gy per fraction, the minimum dose was 0.33 Gy, the maximum dose was 0.62 Gy.

4.4. *Dose measurements*

Cheese phantom, whose density is close to the density of human tissues, was used to measure the doses in the skin layers. The phantom was irradiated with a photon beam of 6 MV energy on a tomotherapy unit. The centering point was in the mid-axis of the long phantom and half the height of the phantom. Points were placed on the surface of the phantom where thermoluminescent detectors were placed during appropriate measurements. Phantom scans were made every 3 mm, which was determined by the size of the phantom markers which were thermoluminescent detectors. The use of the markers and scanning every 3 mm made it possible to calculate the dose at a point for 37 thermoluminescent detectors by the treatment planning system. Six clinical cases were described. Each of them used 37 thermoluminescent detectors based on the coefficient of variation out of 70 used for calibration. Detectors for each clinical case were located at the same measuring points.

5. Results

5.1. *Results of calibration of TLD detectors*

70 thermoluminescent detectors were calibrated as a result of a five-fold calibration procedure. Based on the results obtained from the 5 measurements for each detector, the calibration factor was determined. Determining the calibration factor is necessary to calculate the dose obtained during proper measurements on the Cheese Phantom. The calibration factor is defined as the dose ratio (2 Gy) and the mean calibration measurement. As a result of the calibration, 37 detectors were selected, with a variation factor of less than 3% (except for one detector with a variation factor of 3.38%).

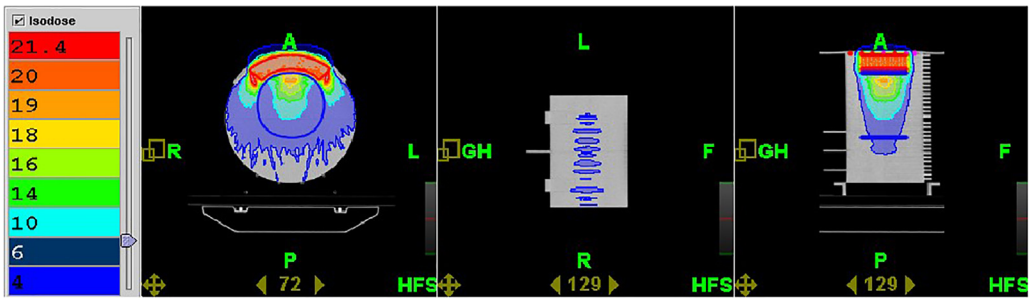

Fig. 3 – Calculated dose distribution for clinical case 1 tumor located at the skin surface using a 0.5 cm bolus.

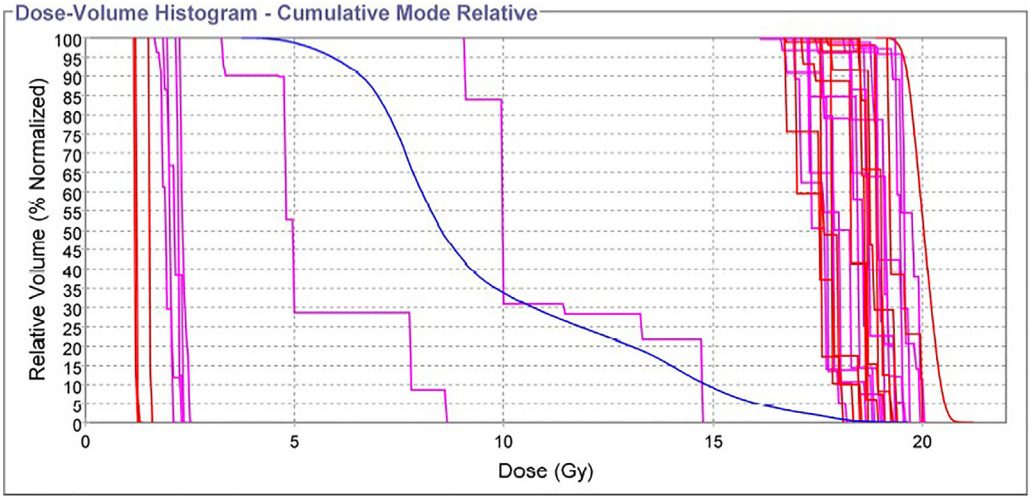

Fig. 4 – Dose volume histogram of dose distribution calculated for clinical case 1: tumor located at the skin surface with 0.5 cm bolus. Numbers 1, 2, 3, 14, 24, 35, 36, 37 indicate detectors outside the irradiation field; Numbers 15 and 23 denote detectors at the boundary of the dose gradients.

5.2. *Dose distributions of calculated doses*

Calculated dose schedules and dose histograms for individual thermoluminescent detectors were calculated by the Hi Art treatment planning system. This system, unlike classical therapeutic treatment systems, differs in that it calculates the dose distribution not only in the patient's body but also in the air, so it is possible to compare the dose measured at the skin surface with the dose calculated at the location of the treatment planning system. Figs. 3 and 4 show an isodose dose distribution and a histogram for clinical case 1: a tumor located just below the skin surface using a 0.5 cm bolus. The dose absorbed through the skin comes from both primary and secondary radiation. For clinical case 1, a more homogeneous distribution was obtained than for clinical cases 3 to 6, due to the shape and location of the tumor just above the skin surface. For Clinical Case # 1, which used a 0.5-cm-thick bolus, a lower dose was obtained for the 1 cm bolus. For a 0.5 cm bolus, the dose distribution is less homogeneous due to the imbalance of electron radiation. Thermoluminescent detectors in this case are located not only in the high dose area, i.e. in the irradiation field, but also at the border and outside the irradiation field.

5.3. *The histogram shows the dose distribution of a single detector and dose*

In the tumor as well as in the critical structure called OAR (Organ At Risk). The curves located at the origin of the coordinate system show a significant deviation from the curves located in the second part of the graph, which is the distribution of the dose points located on the phantom surface in the irradiation field. The dose in the irradiation field is more homogeneous and the average is about 2 Gy. Two curves far out of the others are curves showing the dose distribution of detectors at the target boundary, where large dose gradients occur. The blue curve shows the distribution of the dose in the critical organ.

Figs. 5 and 6 show isodoses as well as a histogram for clinical case 2: lesion located just below the skin surface using a 1 cm bolus. The dose distribution on the skin in this case is more homogeneous than in the tumor lesion located within the patient's body. The detectors are located not only in the high dose area, but also in the area of the irradiation field, on the border and off the irradiated field.

For clinical case 2 for 10 points, the dose distribution differs significantly from the curves in the second part of the

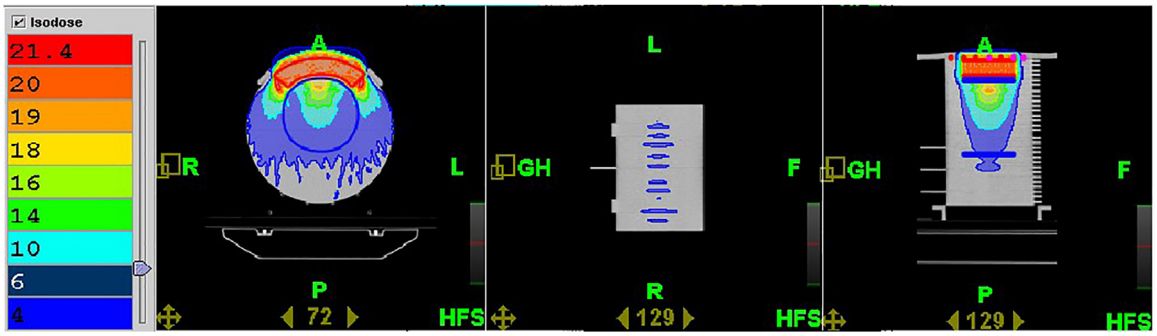

Fig. 5 – Calculated dose distribution for clinical case 2: tumor located at the skin surface with a 1 cm bolus.

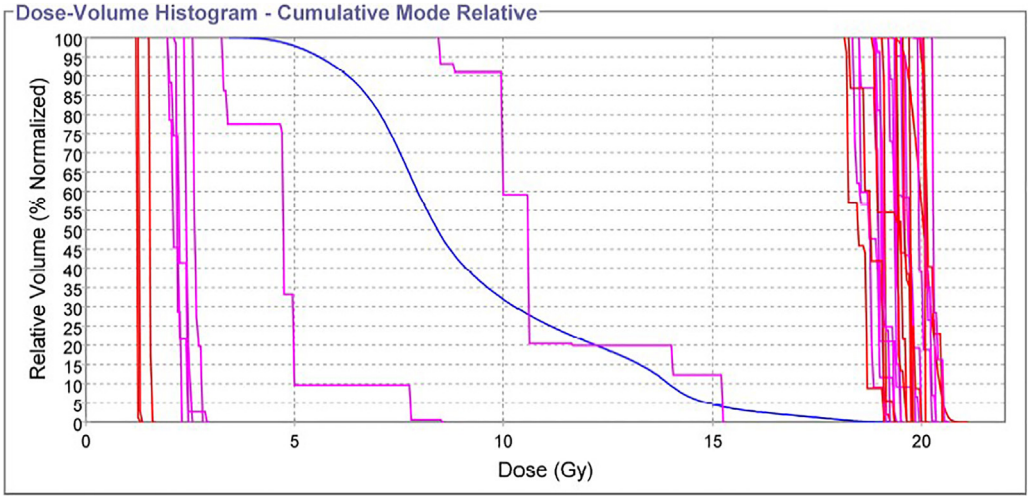

Fig. 6 – Dose volume histogram of dose distribution calculated for case 2: tumor located at the skin surface using a 1 cm bolus. Numbers 1, 2, 3, 14, 24, 35, 36, 37 indicate detectors outside the irradiation field; Numbers 15 and 23 denote detectors at the boundary of the dose gradients.

graph. The curves for points 15 and 23 illustrate the dose distribution for the target and critical target detectors where large dose gradients occur. The points in the irradiation field show a homogeneous dose distribution that is 2 Gy, on average.

Figs. 7 and 8 show isodose distribution and a histogram for clinical case 3: a tumor located within a tissue-like phantom using a 0.5 cm bolus. Detectors in this case were clinically located on the OAR side and were, therefore, outside the radiation field in the low dose region.

On the histogram, the resulting dose distribution is uniform over the tumor location just below the surface of the skin because the detectors were not outside the radiation field in the low dose region. A wider range of doses were obtained in the range of 1 to 7 Gy.

Figs. 9 and 10 show isodose distribution and a histogram for clinical case 4: tumor located within a tissue-like phantom using a 1 cm bolus. In the case of this clinical situation, as in the case of the 0.5 cm bolus, TLD detectors were located in similar dose distribution areas.

The histogram for clinical case 4 is very similar to the histogram for clinical case 3 because of the same location of the tumor and the critical organ. The critical organ was oriented toward the tumor, while the position of the detectors was similar to that of the previous clinical cases. The same detector distribution allows comparison of the dose at the same point for different clinical situations. The use of different bolus thickness results in a more homogeneous distribution of dose, with no curves significantly different from the 5 Gy dose. A dose of 4 to 7 Gy was obtained. For 8 detectors, the dose was calculated to be higher than 5 Gy. The dose was calculated for 10 therapeutic fractions of the patient.

Figs. 11 and 12 show isodose distribution and histogram for clinical case 5: a tumor located within a tissue-like phantom using a 0.5 cm bolus. In this case, the different location of the critical organ that was under the tumor was considered. In this case, the clinical points were located on the lesion side rather than the OAR side. There were high dose gradients in the low dose area near the skin surface.

In clinical case 5 for four measurement points, the dose was lower than for the other points because they were located on the OAR side.

Figs. 13 and 14 show isodose distribution and histogram for clinical case 6: a tumor located within a tissue-like phantom

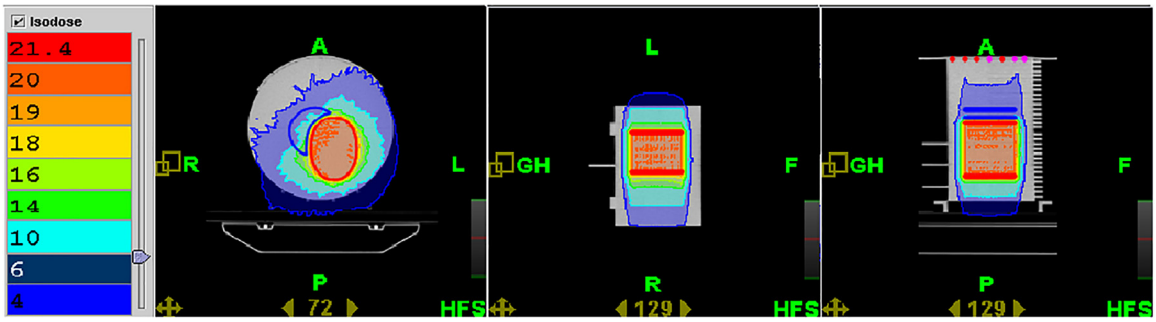

Fig. 7 – Calculated dose distribution for clinical case 3: tumor located within a 0.5 cm bolus.

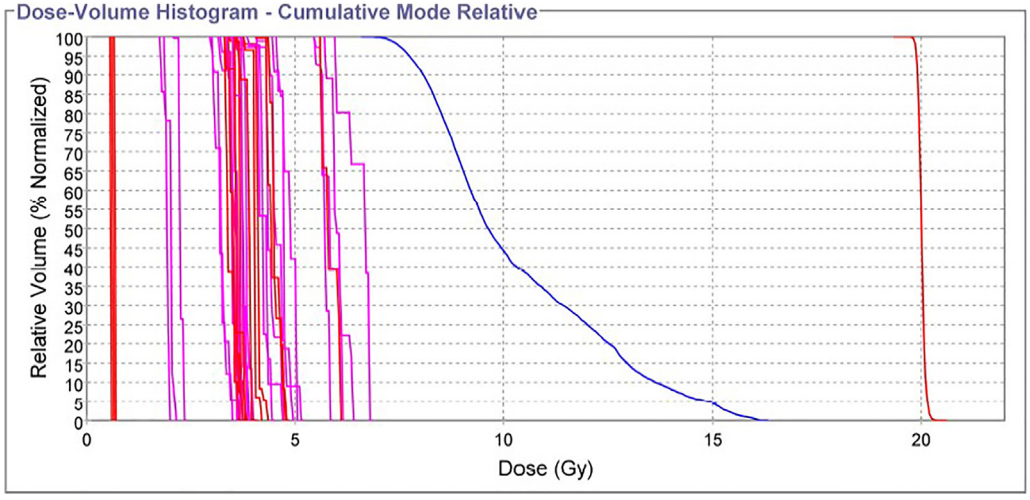

Fig. 8 – Dose volume histogram of dose distribution calculated for clinical case 3: tumor located with a0.5 cm bolus. Numbers 1, 2, 3 indicate detectors outside the irradiation field; Detectors 35, 36, 37 were located out of the range of dose distribution isodoses and 22, 23, 24, 27 in the high dose gradients.

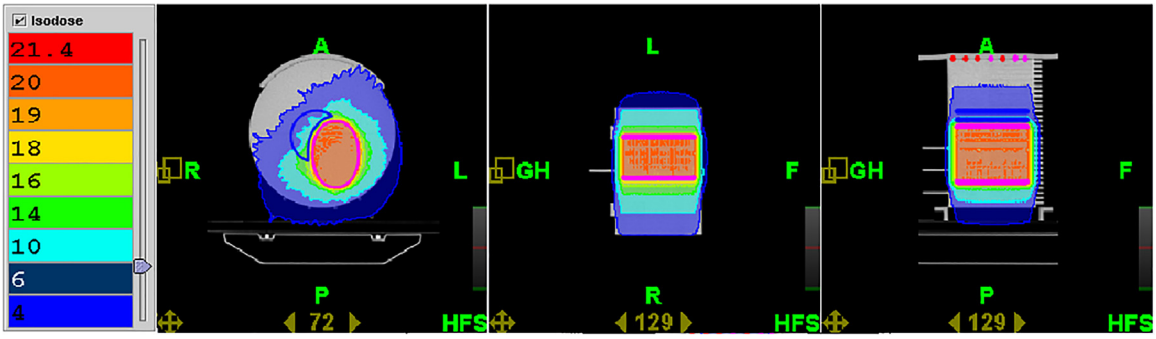

Fig. 9 – Calculated dose distribution for clinical case 4: tumor localized within 1 cm bolus.

using a 1 cm bolus. In this case, like clinical case. 5, large dose gradients appeared in the low dose region at the skin surface.

The histogram for clinical case 6 is analogous to case 5, where 5 measurement points receive a dose of less than 5 Gy. These points are located outside the radiation area.

6. Discussion

Tomotherapy is a spiral irradiation technique, so it is difficult to achieve a homogeneous dose distribution in the skin. On the basis of literature, it can be demonstrated that there is no documented methodology or any reliable results for measuring and verifying the dose in the surface layers of the skin. It is, therefore, necessary to undertake a study to make it possible to specify a method of measuring the dose in the skin, which is difficult due to many factors.

The parameters that affect the accuracy of the dose measurement in the skin include the TLD coefficient of variation and the lack of precise bolus dose optimization due to the presence of airspace between the bolus and the surface of the phantom. The five-way calibration of the detectors

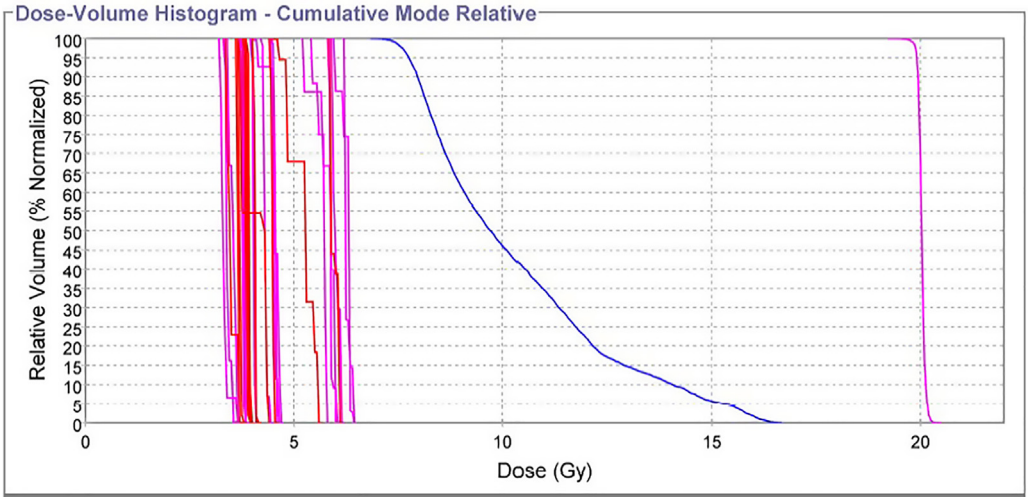

Fig. 10 – Histogram of dose distribution calculated for clinical case 4 tumor located within a 1 cm bolus. Numbers 12, 13, 21, 22, 23, 24, 29, 30 indicate detectors located at the border and outside the irradiation field.

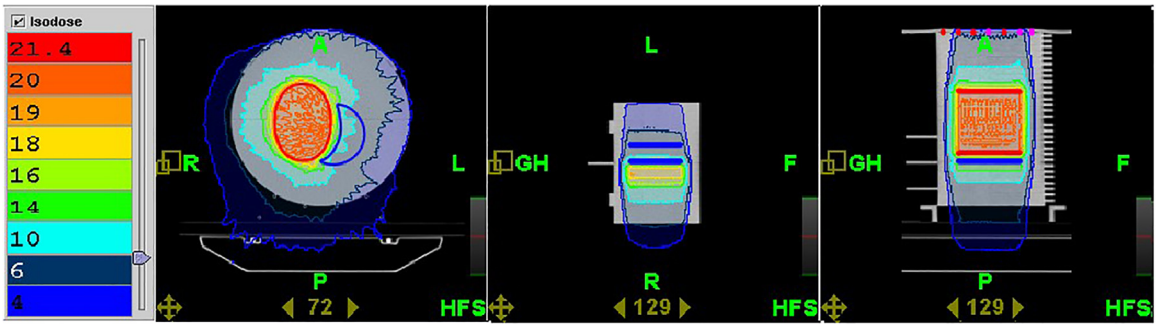

Fig. 11 – Dose distribution calculated for clinical case 5: tumor located within a 0.5 cm bolus.

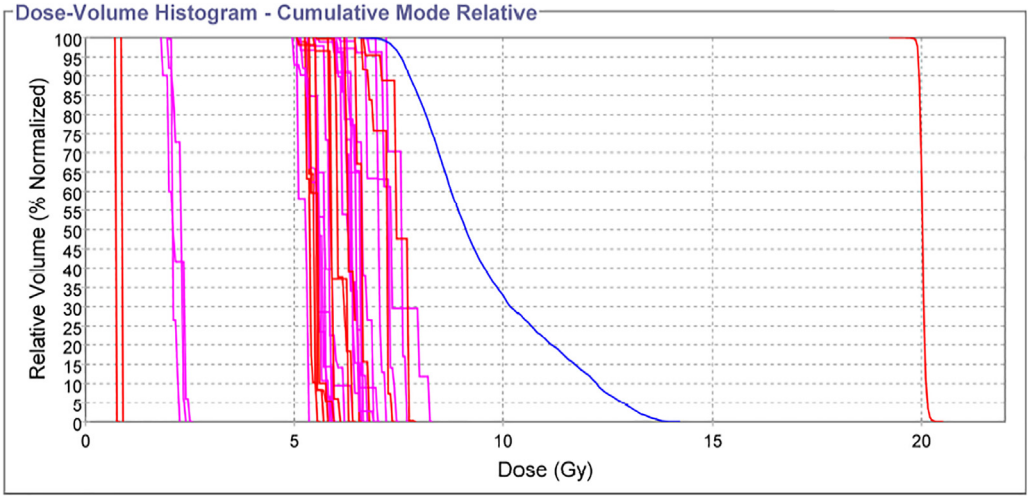

Fig. 12 – Dose volume histogram of dose distribution calculated for clinical case 5: tumor located within a 0.5 cm bolus. Numbers 1, 2, 3 indicate detectors in the high dose gradient region, while detectors 35, 36, 37 are located outside the radiation field.

was designed to demonstrate the repeatability and stability of individual detectors. During calibration, the temperature, pressure and phantom geometry were similar. Based on 5 measurements, one can determine the dispersion of results measured by standard deviation. Stability of the detectors is measured by the dispersion measure: the smaller the variability, the greater the stability of the detectors. The accuracy of the detector means the possibility of obtaining a result which

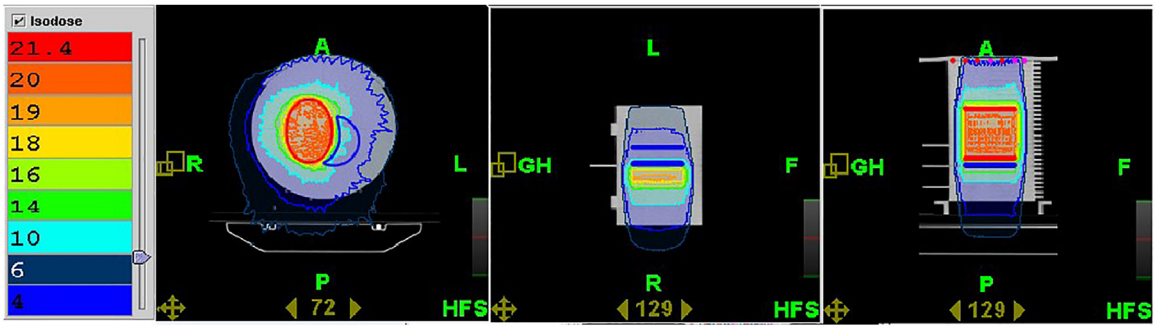

Fig. 13 – Calculated dose distribution for clinical case 6: tumor located within a 1 cm bolus.

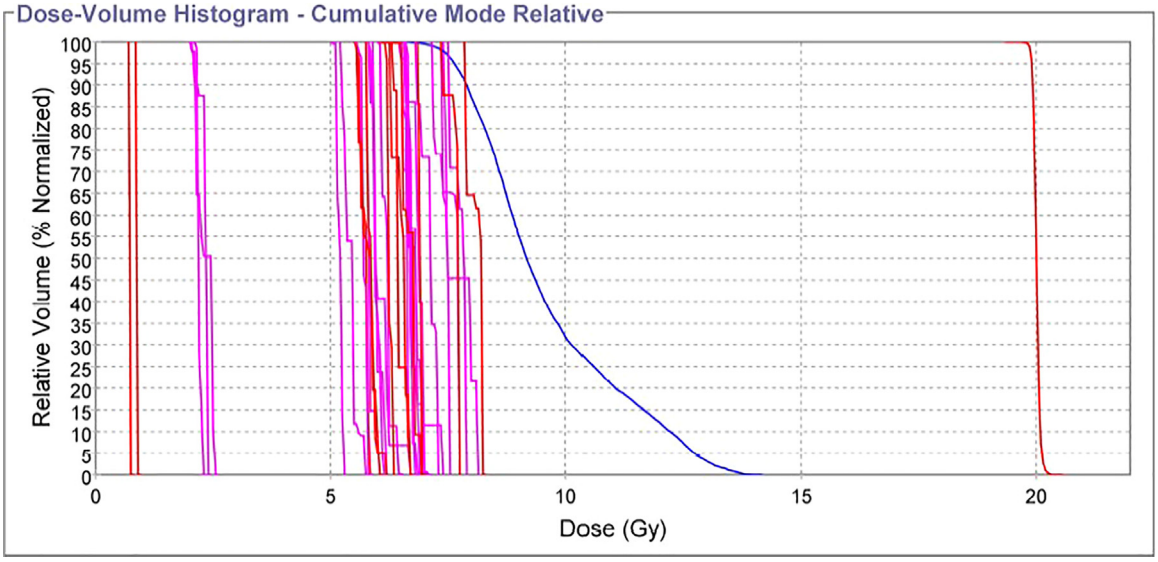

Fig. 14 – Dose volume histogram of dose distribution calculated for internal location using a 1 cm bolus. Numbers 1, 2, 3 indicate detectors in the high dose gradient region, while detectors 34, 35 are located outside the radiation field.

does not differ from the measured value. The smaller the difference between these two values, the more accurate the result.

When comparing doses measured with the planned one, it should be taken into account that the distribution of airspace is different during each therapeutic session, but also with respect to the CT scanned tomography system to form a radiation plan. Figs. 15 and 16 show the location of airspace during phantom irradiation. There are two different situations, depending on the thickness of the bolus used. Bolus is not strictly close to the surface of the phantom, in addition to each fracture, the geometry of the airspace is different for bolus construction.

Another parameter that can significantly influence the comparative study of planned and measured doses is the small size of detectors that cannot be accurately traced in the treatment planning system to calculate the dose in a particular detector. Incorrect tracing of detectors may result in inaccurate dot dosing optimization in the thermoluminescent detector. Due to the dimensions of the detector: 3.0 mm × 3.0 mm × 0.9 mm, a higher resolution system would be needed. Using the current system for contouring structures, it is not possible to precisely contour objects of such small dimensions.

The “plus” or “minus” sign at the percentage difference in dose indicates whether the dose measured by the thermoluminescent detectors was higher or lower than the calculated dose. Differences less than 10% were bolded. Depending on the clinical situation analyzed, this was from 15 to 27 measurement points. The highest compliance, 17 points had a difference of less than 10%, for clinical case 4 where the tumor was located inside the phantom while the critical organ was located on the same side as the detectors. Data analysis shows that the greatest differences occur in points located at the edge of the phantom, where the dose is from 0.08 Gy to 0.3 Gy. Even minor differences in standard deviation in this dose range induce large percentage differences between the planned and measured dose. Also in the area of large dose gradients, i.e. on the OAR-target border, we noticed significant differences between the planned and measured dose.

In order to verify the correctness of the treatment plan, dose measurement in the foresight and low dose region was performed with the A1SL Sn: XW081145 and Sn: XW081146 ionization chamber. Measurement of the chamber showed

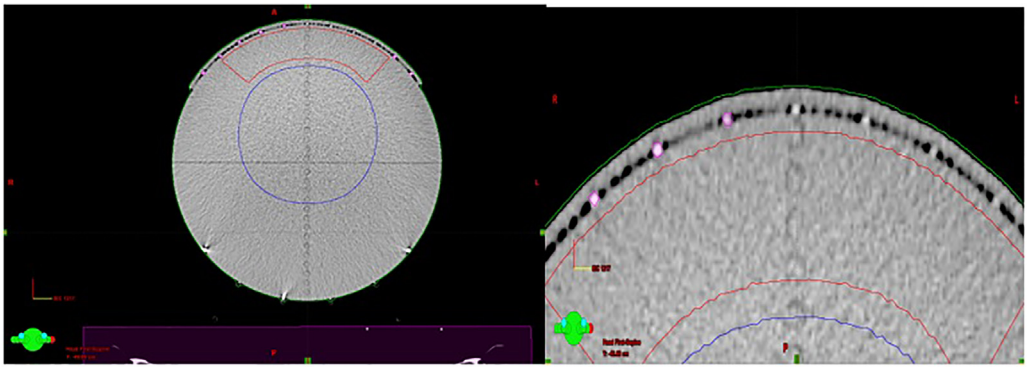

Fig. 15 – Distribution of airspace between a 0.5-cm-thick bolus and the phantom surface.

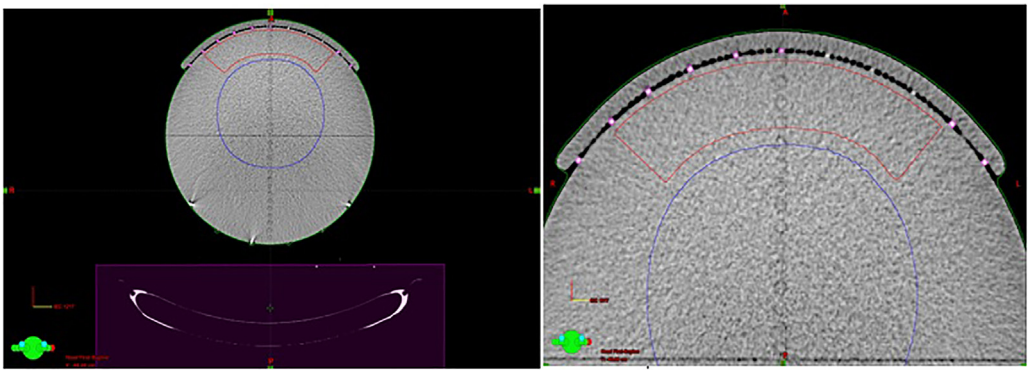

Fig. 16 – Distribution of airspace between a 1-cm-thick bolus and the phantom surface.

Table 2 – Values measured by the ionization chambers for six clinical cases in the low dose region and target. Measurement of the ionization chamber 45 was performed for the target, while the ionization chamber 46, for the low dose region.

Clinical cause	Number of Ionization chamber	$D_{calculated}$ [Gy]	$D_{measure}$ [Gy]
nr 1.	45	2.0	1.95
	46	0.14	0.14
nr 2.	45	2.0	1.97
	46	0.14	0.14
nr 3.	45	2.0	1.97
	46	0.4	0.36
nr 4.	45	2.0	1.98
	46	0.4	0.4
nr 5.	45	2.0	1.96
	46	0.4	0.39
nr 6.	45	2.0	1.98
	46	0.4	0.41

the compliance of the planned and measured dose, which proves the correct implementation of the treatment plan on the therapeutic apparatus. Table 2 shows the results of dose measurements for six clinical cases.

The coefficients of variation of TL detectors calculated on the basis of standard deviation and arithmetic mean were from 0.60 to 4.96%. 70 TL detectors were used for calibration, after detector analysis, detectors with a variation coefficient of more than 5% were discarded. The standard deviation for individual detectors was 0.1–0.6 Gy/C. Detectors with a coefficient of variation greater than 3% could induce a larger measurement error, which is extremely important when measuring such low doses. In the case of a tumor located within the phantom, where the OAR was on the same side as the thermoluminescent detectors at 27 points for a bolus of 1 cm in thickness the difference in dose was 10% lower than in the case with the 0.5 cmbolus. As a result of the analysis in the tissue-like phantom, the average skin-to-skin tumor dose was 1.94 Gy with a 0.5 cm bolus versus 2.03 Gy with a 1 cm bolus. In the case of a tumor located within the phantom and a critical structure located on the same side with the 0.5 cm bolus, the mean dose was 0.66 Gy and for the 1 cm bolus, it was 0.62 Gy. Conversely, when the tumor was located inside the phantom, and the critical structure was located on the opposite side to the detectors. The dose on the skin was 0.75 Gy for the 0.5 cm bolus, and 0.79 Gy for the 1 cm bolus.

Factors contributing to the large difference between the measured and planned dose also included the location of the measurement points in the dose gradient region and the radiation field boundary. In these areas, the verification of the planned does with the measured dose is difficult because a small numerical difference can cause a large percentage difference in the dose, which decreases with the square of the distance. Detectors located at the boundary of dose gradients and at the border of the irradiation field measured low doses, which contributed to the large differences between the planned and measured dose. Buton et al. in their paper entitled "Effects on skin dose from unwanted air gaps under bolus in photon beam radiotherapy" attempted to assess the effect of airspots underneath the bolus during patient irradiation on a classical Linear accelerator. It was attempted to assess what happens to radiation during bolus traction, as well as in the air crevices that form between the patient's bolus and the body or a tissue-like phantom during radiotherapy. The dose in a small air gap under the 1 cm bolus was measured using a ATTIX flat-beam ionization chamber and radiochromic films. During 6 MV energy irradiation using a 1 cm bolus, it was noted that for air crevices up to 2 mm, the dose on the skin did not decrease as demonstrated by the ionization chamber measurements. Four millimeter slots can reduce the dose on the skin by about $0 \pm 4\%$ depending on the size of the field, incidence and other patient-specific parameters. A 1 cm air gap, or bolus thickness, can cause a downward pressure on the skin up to 10% for small irradiation fields and 60° gantry angle. These parameters reduced the dose from 100% Dmax to 90% Dmax. Results from angular measurements showed that with increasing the angle of incidence the dose reduction is increasing, i.e. doses are observed to be lower than planned. Radiochromic film measurements showed the compliance with 2% dose drop measurement for 4 mm slit and 4% for 10 mm slit gap. Clinical studies confirmed that a small air gap between the bolus and the skin of the patient can reduce the dose on the skin, yet 90% of the maximum dose is still delivered to the skin. Only slots above 1 cm can induce a different dose distribution than planned.[2]

The article entitled "Skin dose study of chest wall treatment with tomotherapy" attempted to assess the dose distribution on the skin during thoracic irradiation on a classic accelerator and tomotherapy. Tissue-like bolus is often used to provide the right dose. Tomotherapy is a technique of irradiation that allows a homogeneous dose distribution in PTV. Authors in this experiment hypothesized that getting the right dose on the skin while irradiating the chest wall on tomotherapy will not require a bolus. The study compared the dose on the skin during irradiation on a tomotherapeutic device with that on a classic linear accelerator. Plans for irradiation on tomotherapy were performed with and without a bolus and compared with the results on a conventional accelerator. Plans were also generated on phantoms for primary measurements, doses were measured using MOSFET detectors. The Monte Carlo algorithm was used to optimize the plans. The results showed that higher doses were delivered during tomotherapy than with conventional accelerator irradiation. The dose on the skin increases as the angle of incidence increases.[3]

Kim et al. in his study described dose distribution near the surface durng irradiation on Tomotherapy. In the article "Superficial Dosimetry for Helical Tomotherapy", we investigated the effect of radiation delivery on the skin during spiral Tomotherapy. More precisely, attempts were made to investigate the accuracy of the dose calculation algorithm on the surface of the skin, where the radiation is distributed in an arc rather than perpendicularly. Two types of treatment plans were developed on the Cheese phantom. In the first case, a 2 Gy dose was at the depth of 1 cm of below the surface of the skin. In the other case, the extra dose was 0.5 cm above the phantom surface. The inside of the phantom was completely blocked. EDR2 dosimetry films and TLD detectors were used for dose measurement. From dose distribution measured by dosimetric films, it appears that the skin surface dose was 118.7 cGy in the first case and 130.9 cGy in the other case. Dose measurement with TLD detectors indicated higher scores than those measured with EDR2 due to the thickness of the detectors. In the first case, 95% of the recommended dose was reached at the depth of 2.1 cm. This dose was obtained at the depth of 2.2 cm. The maximum dose was about 110% of the planned dose. As the depth increased, the dose dropped sharply with the above 2 cm depth, 20% of the planned dose was obtained. From the obtained results, it can be concluded that for the depth of 2 cm the system of treatment planning on tomotherapy imprecisely overestimates the dose.[4]

7. Conclusion

Based on the analysis of the obtained results, it was shown that the relative difference between the dose measured and planned in the irradiation field was less than 10%, while the largest differences were observed at the radiation field boundary and off the field where the dose ranged from 0.08 Gy to 1 Gy.

The average dosage in the skin for individual clinical cases was:

A) In the case where the tumor was located on the skin surface, the mean skin dose was 1.94 Gy for a bolus of 0.5 cm in thickness; For a bolus with a thickness of 1 cm, 2.03 Gy.
B) In the case of a tumor located within the phantom and the critical structure on the same side as the thermoluminescent detectors, the average bolus dose in the skin for the bolus was 0.69 Gy and for the bolus 1 cm - 0.62 Gy.
C) When the tumor was inside the phantom and the critical structure was located on the opposite side to the detector, the dose in the skin was 0.75 Gy for the bolus of 0.5 cm, and 0.79 Gy for the bolus of 1 cm.

The coefficient of variation of the thermoluminescent detectors used was less than 3% which made it possible to use them for dose measurement on a tomotherapeutic device.

Air spaces of 1 mm to 4 mm between the bolus and the phantom surface and changing their location during each fraction of irradiation have an influence on the dose distribution in the skin.

Conflict of interest

None declared.

Financial disclosure

We would like to recognize that the Greater Poland Cancer Centre for providing funding grant ref. 19/2016(134).

Uncited references

[6–28]

REFERENCES

1. Łobodziec W. *Dozymetria promieniowania jonizującego w radioterapii*. Katowice: Wydawnictwo Uniwersytetu Śląskiego; 1999.
2. Buton MJ, Cheung T, Yu P, Metcalfe P. Effects on skin dose from unwanted air gaps under bolus in photon beam radiotherapy [w]. *Radiat Measure* 2000;**32**:201–2.
3. Javedan K., Zhang G., Mueller R., Harris E., Berk L, Forster K., Skin dose study of chest wall treatment with tomotherapy [w]: Jpn J Radiol Volume 27, Number 9, 355-362, DOI: 10.1007/s11604-009-0357-9.
4. Kim Song Yih, You Sei Hwan, Song Taesoo, Kim Yong Nam, Keum Ki Chang, Cho Jae Ho, Lee Chang Geol, Seong Jinsil. Superficial dosimetry for helical tomotherapy [w]. *J Korean Soc Ther Radiol Oncol* 2009;**27**(2):103–10.
5. http://www.standardimaging.com/product_home.php?id=26.
6. Gorączko W. *Radiochemia i ochrona radiologiczna*. Poznań: Wydawnictwo Politechniki Poznańskiej; 2003.
7. Pruszyński B. *Radiologia, Diagnostyka obrazowa, nowe wydanie*. Warszawa: Wydawnictwo lekarskie PZWL; 2003.
8. Rudnicki T. *Podstawy radiobiologii medycznej*. Poznań: UM im. Karola Marcinkowskiego w Poznaniu; 1984.
9. Scharff W. *Akceleratory biomedyczne*. Warszawa: Wydawnictwo Naukowe PWN; 1994.
10. Johns HE, Cunningham JR. *The physics of radiology*. Illinois: Springfield; 1983.
11. http://www.euronuclear.org/info/encyclopedia/i/ionizationchamber.htm.
12. Niewiadomski T. *Fluorek litu i jego zastosowanie w dozymetrii (promieniowania jonizującego)*. Warszawa: Ośrodek informacji o energii jądrowej; 1986.
13. Podgorsak EB. Treatment machines for external beam radiotherapy. In: Podgorsak EB, editor. *Radiation oncology physics*. Vienna: International Atomic Energy Agency; 2005.
14. Mackie TR. History of tomotherapy. *Phys Med Biol* 2006;**51**(13):442.
15. Mackie TR, Holmes TW, Swerdloff S. Tomotherapy: a new concept for the delivery of conformal radiotherapy. *Phys Med* 1993;**20**:1709–19.
16. *On the Role of Helical Tomotherapy in Clinical Practice: Results from Planning Studies*, In London Health Sciences Centre and Ontario Canada University of Western Ontario, London, editors, *Integrated Cancer Program*, 2004.
17. TomoTherapy Incorporated. *TomoTherapy Hi·Art Physics Verification*; 2007.
18. Kissick MW, Fenwick J, James JA, Jeraj R, Kapatoes JM, Keller H, Mackie TR, Olivera G, Soisson ET. The helical tomotherapy threadeffect [w]. *Phys Med* 2005;**32**(5):1414–23.
19. Shepard DM, Olivera GH, Reckwerdt PJ, Mackie TR. Iterative approaches to dose optimization in tomotherapy[w]. *Phys Med Biol* 2000;**45**(1):69–90.
20. http://www.standardimaging.com/product_home.php?id=26.
21. Van Dyk J, Kron T, Bauman G, Battista JJ, Tomotherapy: A Revolution In Radiation Therapy, London Regional Cancer Centre, University of Western Ontario.
22. Stanisz A. *Przystępny kurs statystyki z zastsowaniem Statistica na przykładach z medycyny Tom 1*. Kraków: StatSoft; 2006.
23. TomoTherapy Incorporated. *TomoTherapy Hi·Art Physics Verification* 2007.
24. Akademia Górniczo-Hutnicza im. S. Staszica w Krakowie Wydział Fizyki i Informatyki Stosowanej, *Dozymetria Termoluminescencyjna, Instrukcja do ćwiczenia laboratoryjnego z dozymetrii promieniowania jonizującego dla studentów specjalności Fizyka Medyczna i pokrewnych*, WFiIS AGH.
25. Ryczkowski A. Metody optymalizacji rozkładu dawki w radioterapii realizowanej przy użyciu aparatu tomoterapeutycznego, Praca magisterska. *Wydział Fizyki Uniwersytetu im. A. Mickiewicza w Poznaniu* 2009.
26. Ryczkowski A, Piotrowski T. Tomotherapy archive structure and new software tool for loading and advanced analysis of data contained in it [w]. *Reports of Practical Oncology and Radiotherapy* 2011;**16**(2):58–64. March-April, Pages.
27. Piotrowski T., Martenka P., de Patoul N., Jodda A., Coevoet M., Malicki J., Vynckier S., *The new two-component conformity index formula (TCCI) and dose-volume comparisons of the pituitary gland and tonsil cancer IMRT plans using a linear accelerator and helical Tomotherapy* [w]: Reports of Practical Oncology and Radiotherapy, Volume 14, Issue 4, Pages 133-145.
28. Malicki J, Kornafel J. *Podstawy fizyczne i radiologiczne radioterapii [w]: Ginekologia onkologiczna (pod red.) Markowska J, wyd*; 2006, 2, t.l, Wrocław.